Journal of Hydrology: Regional Studies 15 (2018) 90–104

Contents lists available at ScienceDirect

Journal of Hydrology: Regional Studies

journal homepage: www.elsevier.com/locate/ejrh

Hydrometeorology of the catastrophic Blanco river flood in South Texas, May 2015

Chad Furl[a,*], Hatim Sharif[a], Jon W. Zeitler[b], Almoutaz El Hassan[a], John Joseph[a]

[a] University of Texas at San Antonio, Department of Civil Engineering, One UTSA Circle San Antonio, TX, 78249, United States
[b] NOAA/National Weather Service, Austin-San Antonio Weather Forecast Office, 2090 Airport Rd New Braunfels, TX, 78130, United States

ARTICLE INFO

Keywords:
Flood hydrology
Texas hill country
Blanco river
GSSHA
Hydrometeorology

ABSTRACT

Study region: This study was carried out along the Blanco River in south-central Texas which drains approximately 1100 km^2.
Study focus: Unprecedented rainfall across the state of Texas in May 2015 produced flooding that claimed at least 24 lives across the state. The most devastating single event over this period occurred on 23–24 May along the Blanco River, where a fast moving floodwave resulted in eleven fatalities in the town of Wimberley. The storm event resulted in the flood of record at the USGS gauge in Wimberley which has collected data since the 1920s.
New hydrological insights: Meteorological observations, high-resolution rainfall estimates, and physics-based distributed hydrological modeling provide the opportunity to examine the hydrometeorological mechanisms accompanying the extreme storm and subsequent flood. Additionally, transpositions of the radar rain fields forced through the hydrologic model allow for analysis of the effect of position of the centroid of the storm relative to the catchment on floodwave propagation. Two major controls on the flood response are identified and analyzed: the position of heavy storm cells over the headwaters with subsequent slow movement downstream and the extremely moist antecedent conditions prior to the onset of the event.

1. Introduction

The year of 2015 brought unprecedented rainfall to the state of Texas. Statewide precipitation records were set for calendar year (1047 mm), four month (March–June, 513 mm), three month (April–June, 425 mm), two month (April–May, 330 mm), and one month (May, 230 mm) (NOAA, 2016). The abnormally wet spring ended a 5-year drought across the state. By mid-July 2015, no areas in the state were classified in D1-D4 drought conditions, compared to 45% at the beginning of the year (United States Drought Monitor, 2015). From January–June 2015 water supply reservoirs increased in capacity from 63% to 84% at monitored reservoirs statewide (Texas Water Development Board, 2015). In addition to the unusually large amount of rainfall, spring 2015 will be remembered for numerous severe weather outbreaks across the state, producing hail storms, tornadoes, and several impactful flood events. Severe flooding occurred in several areas of the state including the major urban areas of Dallas, San Antonio, Austin, and Houston.

While the unusually persistent statewide rainfall was rare, the occurrence of severe floods in Texas were not. The central portion of Texas is particularly disposed to flash floods due to the combination of flood prone physiography and susceptibility to extreme rainfall events (Ashley and Ashley, 2008). The region has produced some of the largest rainfall events and flood magnitudes in the

* Corresponding author. Current address: The Edwards Aquifer Authority. 900 E Quincy San Antonio, TX 78215, United States.
E-mail address: Chad.Furl@gmail.com (C. Furl).

https://doi.org/10.1016/j.ejrh.2017.12.001
Received 29 May 2017; Received in revised form 17 October 2017; Accepted 1 December 2017
Available online 15 December 2017

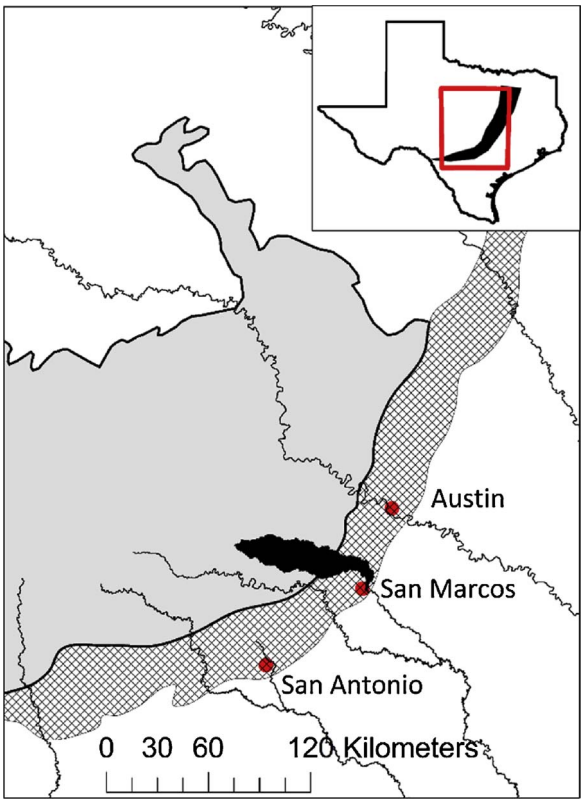

Fig. 1. Study area map. The solid filled shape indicates the Blanco River watershed at its confluence with the San Marcos River. The solid grey area is the Edwards Plateau and Llano uplift ecoregions comprising the "Texas Hill Country". The cross hatched area is the Balcones Fault zone. The red dots are the cities of San Antonio, San Marcos, and Austin. The black shaded region in the upper right hand corner area map represents the approximate delineation of "Flash Flood Alley". (For interpretation of the references to colour in this figure legend, the reader is referred to the web version of this article.)

United States and world (Baker, 1975; Smith et al., 2000). This region of Texas extending from San Antonio north through Dallas has been dubbed "Flash Flood Alley" (FFA) and has been identified as one of the most dangerous areas in the United States for flash flooding (Burnett, 2008; Zahran et al., 2008; Sharif et al., 2012; Sharif et al., 2014).

Much of the severe flash flooding along FFA occurs in the southern portion of the region along the Balcones Escarpment and Texas Hill Country region (Fig. 1) (Smith et al., 2000; Ashley and Ashley, 2008). The Balcones Escarpment bounds FFA to the west and separates the limestone terrain of the Edwards Plateau from the gently sloping clay terrain of the Blackland Praries. The landscape in this area is characterized by very thin soils, exposed bedrock, and steep surfaces promoting runoff (Patton and Baker, 1976; Baker, 1977; Costa, 1987; Wilcox et al., 2007). It has traditionally been thought that high magnitude rainfall events occurring in this region can be enhanced orographically from the Escarpment and Hill Country topography (Baker, 1975; Caracena and Fritsch, 1983; Caran and Baker, 1986; Nielsen-Gammon et al., 2005; Burnett, 2008; Furl et al., 2015), although recent work by Nielsen et al. (2016) suggests orographic effects are minor. Regardless, rainfall and runoff extremes delineating the Texas envelope curve primarily occur along the Edwards Plateau/Balcones Escarpment area (Asquith and Slade, 1995).

On May 23–24, 2015, one of the most lethal flash floods in Texas history occurred along the Blanco River in the Texas Hill Country. The event occurred over the holiday weekend of Memorial Day at this popular tourist destination for river recreation. Eleven individuals perished in the vicinity of Wimberley, TX (personal communication − Wimberley City Manager) as the floodwave swept away homes. Hundreds of high water rescues were conducted by emergency personnel in the aftermath of the flood. The flood destroyed several hundred homes in the floodplain and caused severe infrastructure damage including two bridge washouts. The area was declared a federal and state disaster area.

Several studies have been conducted over the last several years examining the physical controls of major flood events across the Texas Hill Country (e.g. Vieux et al., 2004; Sharif et al., 2010a; Sharif et al., 2010b; Looper and Vieux, 2012; Elhassan et al., 2013; Sharif et al., 2013; Chintalapudi et al., 2014; Furl et al., 2015). These studies combine remotely sensed precipitation products with fully distributed, physics based hydrological (PBD) models. PBD hydrological models solve sets of partial differential equations across a gridded mesh allowing for spatially explicit detail in describing the interaction between rainfall and land surface properties.

In addition to examining watershed processes or conducting post-event investigations, PBD models can be used for hydrologic forecasting in an operational setting when forced with quantitative precipitation estimates (QPE) or quantitative precipitation forecasts (QPF) (Looper and Vieux, 2012). QPEs have the benefit of using real time radar volume scans, but their maximum lead time for flood prediction is equal to or less than the basin's time of concentration. This can limit their utility in basins such as those found

in the Texas Hill Country which are known to respond quickly to rainfall. QPFs provide greater lead times for flood forecasting at the cost of accuracy (Sharif et al., 2006; Vivoni et al., 2007; Collier, 2007).

In the present study, we describe the succession of hydrometeorological events leading up to and resulting in the Blanco River flood. We examine the synoptic scale (e.g., Wang et al., 2015) and mesoscale weather patterns leading to the development of catastrophic rainfall and detail the structure, motion, and evolution of rainfall across the basin. The flood hydrology of the event is examined through PBD hydrological modeling with the Gridded Surface Subsurface Hydrologic Analysis (GSSHA) model (Downer and Ogden, 2004). Lastly, the effect of storm location and precipitation amount on peak flows are examined by model iterations transposing rainfall fields across different areas of the basin. Implications for flash flood forecasting are discussed. Our analysis is divided into separate sections discussing 1) Storm Properties, 2) Basin Rainfall, 3) Flood Hydrology, and 4) Rainfall Transpositions. We begin with a description of the drainage basin, methods of analysis are reported as they are discussed throughout.

2. Area description

The Blanco River watershed encompasses approximately 1100 km^2 at its confluence with the San Marcos River in south-central Texas. The watershed is oriented in an east-southeast direction, and forms the northern headwaters of the larger Guadalupe River system which flows to the Gulf of Mexico. The Colorado system bounds the watershed to the north and upper Guadalupe to its south (Fig. 1).

The Blanco River extends approximately 75 km through the karst landscape of the eastern Edwards Plateau before flowing past the Balcones Escarpment in the lower portion of the watershed. The surface geology west of the Balcones Escarpment mainly consists of lower Cretaceous limestones resulting in a rugged surface. Soils in this area are thin (< 1 m). East of the escarpment, surface geology primarily consists of nonresistant Upper Cretaceous limestones resulting in flat terrain. There is significant surface water – groundwater interaction throughout the main stem of the river. At normal to dry conditions, the Blanco contains long stretches of dry stream bed and stagnant pools. Under extreme drought, the river flows for only about half its length. Much of the stream flow under low flow conditions originates from the Pleasant Valley Spring and Jacobs Well Spring (Fig. 2). Flow entering sinks along the channel

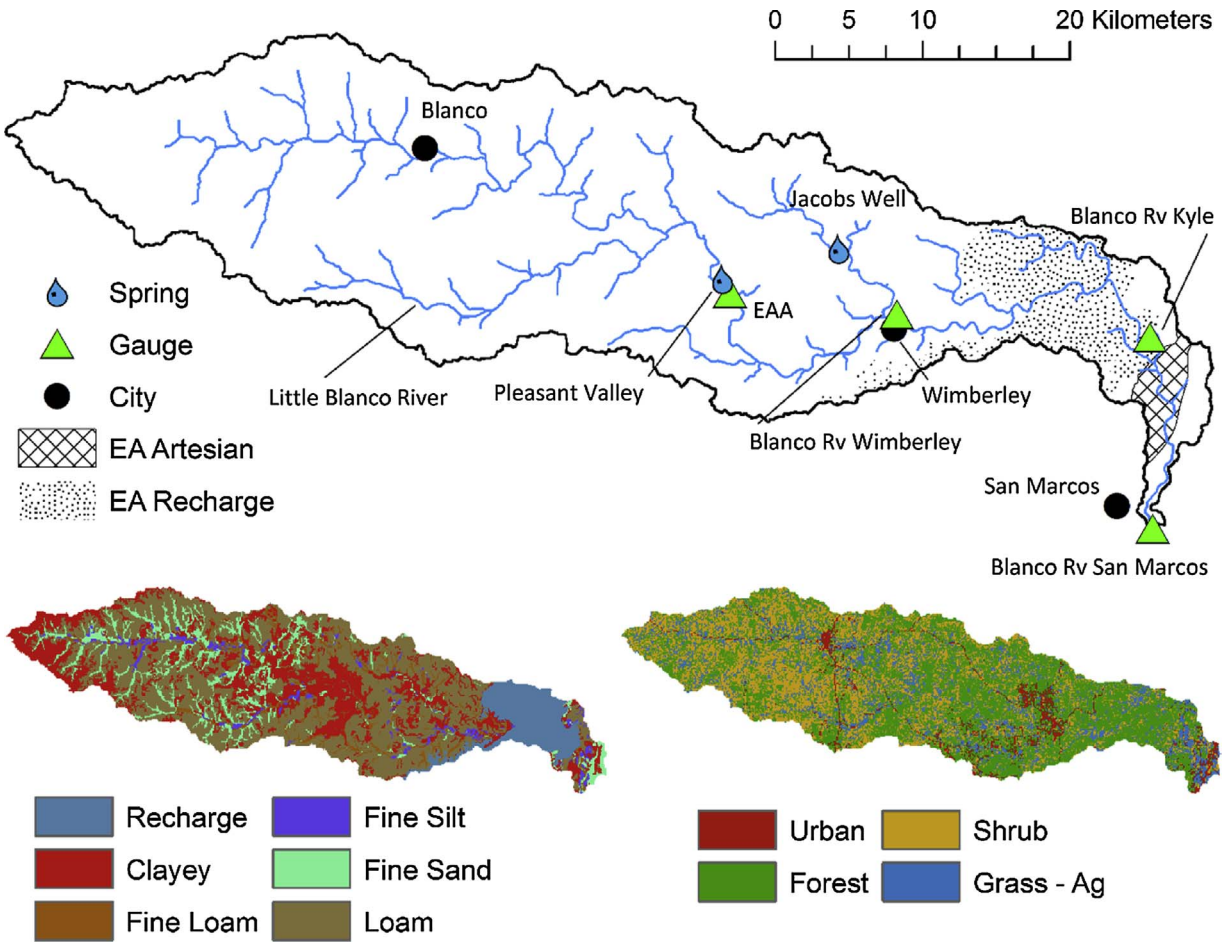

Fig. 2. The Blanco River watershed with key hydrologic features (top). Generalized soils (bottom left), and land use maps (bottom right).

have been dye traced to Barton Springs approximately 50 km north east (Grimshaw and Woodruff, 1986; Collins 2004; Smith et al., 2014; Smith et al., 2015).

The Blanco River basin is sparsely populated with the small communities of Blanco and Wimberley (< 3000 persons each) located along the river. Near the outlet, the larger sized city of San Marcos intersects a portion of the basin. Land use in the basin is primarily fallow land along with areas cleared for ranching purposes. Vegetation in undeveloped areas of the watershed is a mix of oak, juniper, mesquite, and grasses. Riparian areas are dominated by bald cypress, oak, elm, cedar, and conifers. Soil texture and land use maps are shown in Fig. 2.

Climate in the study area is classified as subtropical humid with short mild winters and hot summers. The region is prone to frequent droughts which can be severe and persist for months or years (e.g. Nielsen-Gammon and William, 2012). Spring and Fall are the wettest seasons with average annual rainfall in the area of about 770 mm (NOAA, 2016). The majority of rainfall can be attributed to passage of continental fronts, mesoscale convective systems (MCSs) (e.g. Smith et al., 2000; Nielsen-Gammon et al., 2005), and localized convective events during warmer months resulting in short-duration high intensity events. Occasionally, tropical disturbances protrude far enough inland resulting in major precipitation events (Asquith and Slade, 1995).

3. Storm description

Aspects of the storm that produced flooding within the Blanco River are examined through analysis of synoptic and mesoscale features leading to, and evolving during, the event. Rainfall generating the floodwave fell during the overnight and early morning hours of 23 May – 24 May 2015. Approaching from a synoptic scale viewpoint, GOES water vapor image at 1745 UTC 23 May (Supplementary Fig. A1), right at the onset of deep moist convection over south central Texas. Wang et al. (2015) outline a preferred wave-train pattern across North America, resulting from a strengthened teleconnection with El Niño, that enhances positive water vapor flux and upper-jet upward motion across the southern Great Plains. The translation of the mean longwave pattern to the specific event of 23–24 May in the water vapor imagery (Supplementary Fig. A1) shows a longwave trough centered over the southern Rockies, upper level jet streak (pink/red shading), and evident taps to moist air from the Pacific and Gulf of Mexico (gray/white shading). An associated shortwave trough axis over the Mexican states of Sonora and Chihauhua is poised to move into West Texas. All of these features support water vapor flux and/or general upward vertical motion across Texas.

In fact, the 300-hPa Rapid Refresh (RAP) upper air objective analysis for 0000 UTC 24 May 2015 (Fig. 3) shows the right entrance

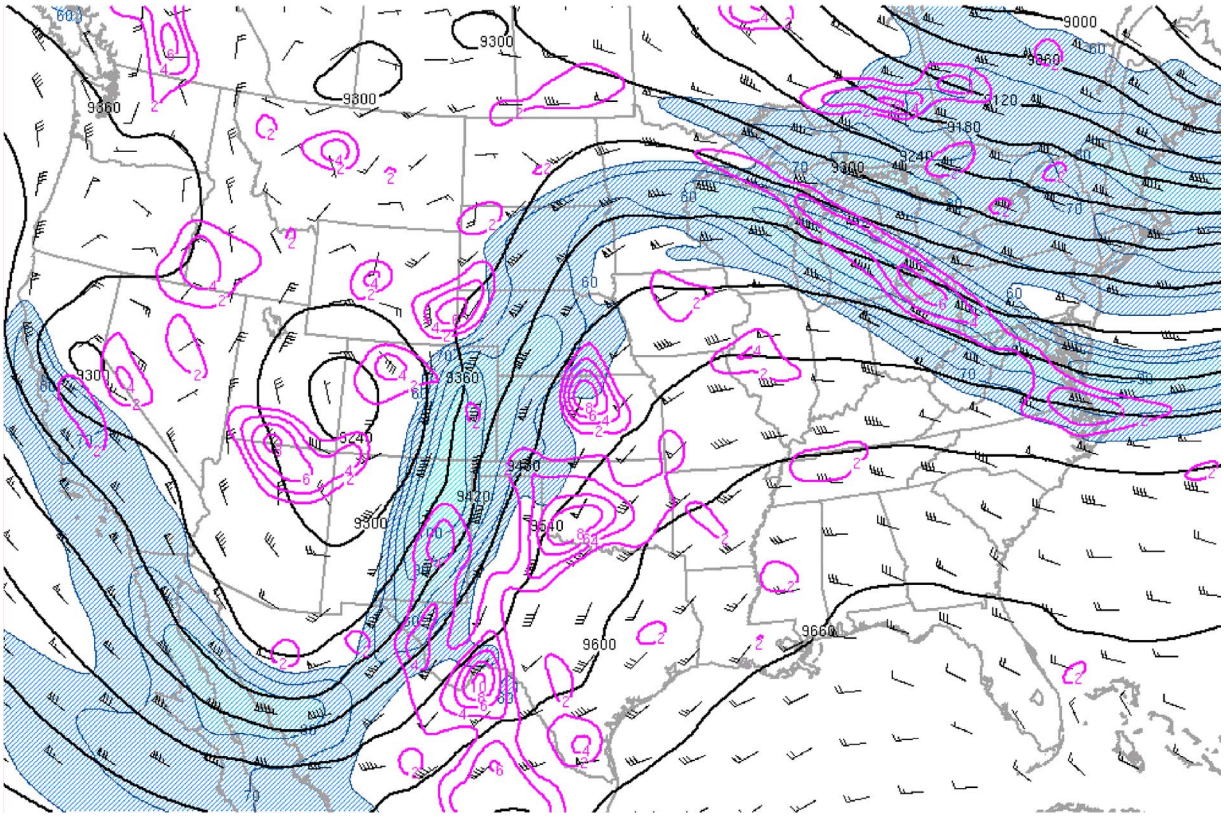

Fig. 3. 300-hPa modified RAP analysis for 0000 UTC 24 May 2015 showing geopotential height (m, black), wind barbs (kts, black), isotachs (shaded above 30.9 ms^{-1}, blue), divergence (10^{-5} s^{-1}, pink). Courtesy of NOAA/NWS/Storm Prediction Center (2016). (For interpretation of the references to colour in this figure legend, the reader is referred to the web version of this article.)

region to a jet streak over the Texas Big Bend region, with strong divergence across that area and extending into south central Texas. Supplementary Fig. A2 shows aligned kinks in the 500-hPa RAP analysis height field in northern Mexico and the Texas Big Bend region, indicative of a weak shortwave trough that would pass from southwest to northeast across Texas in moderate to strong southwesterly flow (note shaded 20.6 ms^{-1} or greater winds). Continuing downward to 850 hPa, Supplementary Fig. A3 shows strong moist advection from the Lower Rio Grande Valley throughout Texas (10–15 ms^{-1} winds and dark green 14 °C dewpoint). Similarly, Supplementary Fig. A4 depicts the surface pattern, with implied moist advection via southerly winds from the Gulf of Mexico inland toward a low pressure in eastern New Mexico. These constituent patterns did not change appreciably during the event, other than the mid-level shortwave trough progressing to the northeast across Texas. They match fairly close to the mesohigh-type heavy rainfall pattern documented in Grice and Maddox (1983), placing the target area for subsequent heavy rainfall over south central Texas.

In addition to the synoptic/pattern-based analysis by Grice and Maddox (1983), Doswell et al. (1996) present an ingredients-based approach that is more focused on mesoscale aspects of heavy rain production. Examination of the precursor environment through a proximity upper air sounding indicates key ingredients were in place for heavy rain. In Supplementary Fig. A5, a 0000 UTC 24 May 2015 RAP analysis sounding from Austin-Bergstrom International Airport (KAUS) has a precipitable water value of 49.8 mm, over two-standard deviations above the mean value for May in south central Texas. The warm cloud depth defined from the lifting condensation level (LCL) to −10 °C level, after Schroeder et al. (2016) is between 4.5 and 5 km, while moderate CAPE of 1855 J kg^{-1} is well-distributed throughout the profile, along with the environmental lapse rate close to moist adiabatic, with a high relative humidity throughout (mean of 91%). Individual cell storm motion could be assumed to be with the 0–6 km mean wind, 190° at 15.9 ms^{-1}, however, *meso*-beta scale (Orlanski, 1975) convective elements (MBEs, Corfidi et al., 1996) would be nearly orthogonal and slower (260° at 7.2 ms^{-1}). Thus, the environment supported deep, moist convection and heavy rain, especially given the high precipitable water and large warm cloud depth supporting collision-coalescence rain processes. While the moderate cell motion would typically be a mitigating factor for heavy rain, the nearly orthogonal and slow MBE motion, and moderate shear could support cell-training over localized areas, and hence heavy rainfall.

Mesoscale model (especially the High Resolution Rapid Refresh, Benjamin et al., 2016) runs indicated organized convection 18–24 h prior to the event in the form of a Mesoscale Convective System (MCS) developing over the Texas Big Bend region and propagating east across south central Texas. Sequential NEXRAD radar reflectivity (Fig. 4) shows the models verified well from a qualitative perspective. What the models did not forecast was the development and propagation of a *meso*-gamma (Orlanski, 1975)

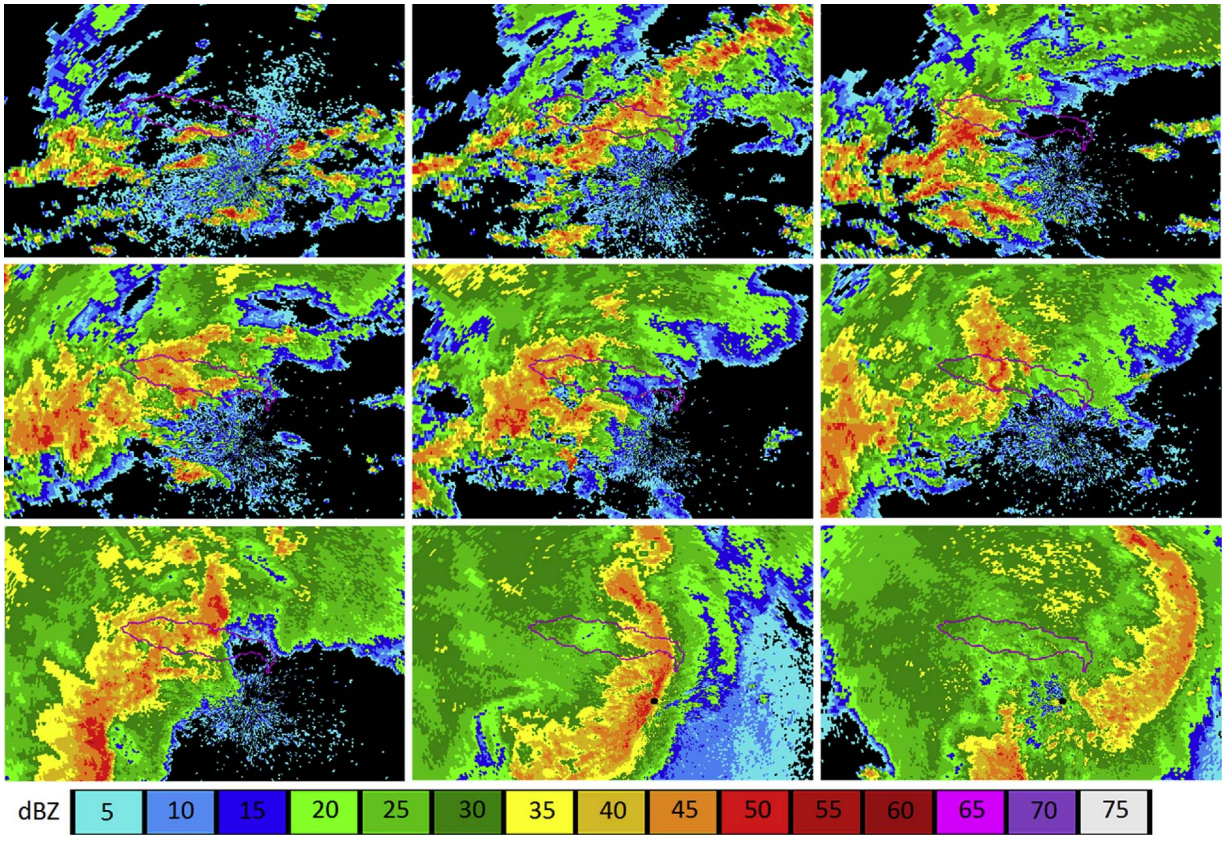

Fig. 4. Level II NEXRAD reflectivity images (0.5° angle) from KEWX at the top of each hour from 1900 UTC 23 May 2015 to 0300 24 UTC May 2015 (left to right, top to bottom). The Blanco River watershed is pictured.

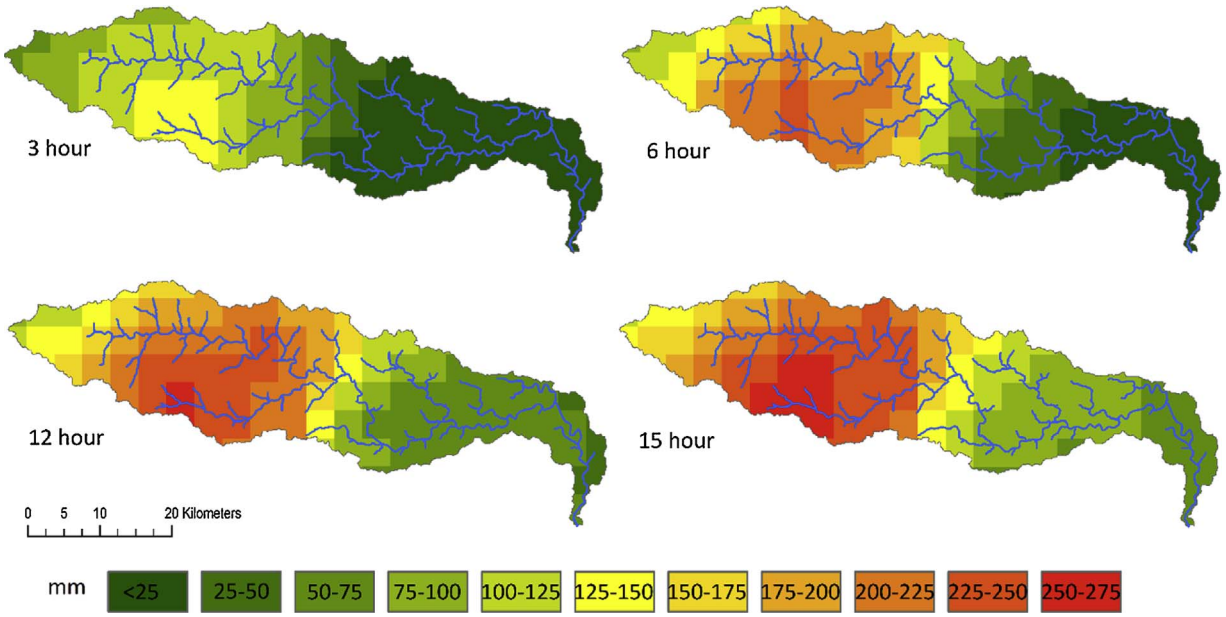

Fig. 5. Maximum rainfall accumulations developed from stage IV data for 3, 6, 12, and 15 h time periods.

convective vortex, which propagated along the mean wind and merged with the northern bookend vortex of the MCS around 0100 UTC on 24 May 2015 (lower left panel of Fig. 4). This merger maintained heavy rainfall over the upstream, western end of the Blanco River basin, followed by the MCS propagating eastward (and down basin), potentially providing additional flow as the main floodwave also moved downstream. Flash flood guidance values generated by the National Weather Service West Gulf River Forecast Center were well below normal (43 mm in 1-h, 58 mm in 3-h, and 76.2 mm in 6-h) due to rainfall in the preceding two weeks that resulted in increased soil moisture, and hence would result in initial flash flooding being observed at lower rainfall rates. However, NEXRAD and estimated rainfall in excess of 220 mm in the upper Blanco River basin, easily exceeded these values.

4. Rainfall

The synoptic and mesoscale setup resulted in widespread heavy rainfall across the Texas Hill Country. The event lasted approximately 15 h across the Blanco River watershed from 1900 UTC 23 May 2015–1000 UTC 24 May 2015 with a general west to east flow across the Hill Country region. Fig. 4 shows raw Level II radar reflectivity (lowest angle) scans from the top of each hour (1900 UTC 23 May 2015–0300 UTC 24 May 2015) along with the Blanco River watershed. Rainfall producing the floodwave along the Blanco River occurred primarily in the seven hour period between 1900 UTC 23 May 2015–0200 UTC 24 May.

Rainfall accumulations across the basin were examined using the NWS/NCEP stage IV QPE product (herein stage IV) (Lin and Mitchell, 2005). The precipitation estimate is a quality controlled multi-sensor product (radar and gauges) produced by NCEP from the NEXRAD Precipitation Processing System (Fulton et al., 1998) and the NWS River Forecast Center precipitation processing (Nelson et al., 2015). Precipitation bins are 4 km × 4 km and have an hourly time step. A basin-wide hyetograph derived from the stage IV precipitation data are shown in Supplementary Fig. A6. The 1100 km^2 watershed averaged about 165 mm during the 15 h maximum, with about 130 mm of precipitation falling over the wettest 7 h. Fig. 5 displays accumulations for maximum 3, 6, 12 and 15 h totals.

A key feature of the storm was it remaining nearly stationary over the headwaters of the Blanco River. During the seven hour period of maximum rainfall, strong radar echoes (> 50 dBZ) were present in the upper half of the basin upstream of the confluence of the Blanco and Little Blanco Rivers. When the strongest cells moved off of the headwaters they followed the course of the river downstream. Supplementary Fig. A6 displays a rainfall hyetograph for the area delineated at the confluence of the Blanco and Little Blanco Rivers. This 615 km^2 area (approximate upper half of the watershed) received event totals of approximately 220 mm. This area of the basin is characterized by steep channel beds and steep topography forming narrow valleys and channels. Downstream areas heavily impacted by the floodwave received much less rainfall (25–75 mm). The lack of extreme rainfall in the lower, populated, portion of the basin was a missing environmental cue to the potential of a flood wave coming downstream, and may have slowed evacuation response, exacerbating the death toll from the event.

Rainfall return periods were calculated at 1, 3, 6, and 12 h intervals from the stage IV bin containing the highest accumulation for each time period. Return periods were calculated following the methods of Asquith (1998) which employs a regionalization approach for the state of Texas utilizing a generalized logistic (GLO) distribution. Asquith (1998) concluded the GLO distribution was more appropriate than the generalized extreme value distribution for storm durations up to 24 h. The storm's point annual nonexceedance probability (F) is estimated by:

Table 1
Recurrence Intervals for stage IV and CoCoRaHS precipitation measurements.

Rainfall measurement – Duration	Precipitation (mm)	Recurrence interval (year)
Stage IV bin max 1 h	63.8	10
Stage IV bin max 3 h	149.6	90
Stage IV bin max 6 h	245.1	320
Stage IV bin max 12 h	261.1	200
CoCoRaHS assumed 12 h	304.8	380
CoCoRaHS actual 24 h	304.8	270

$$F = \frac{1}{1 + \left\{1 - \frac{\kappa}{\alpha}[X_d(F) - \xi]\right\}^{\frac{1}{\kappa}}} \quad (1)$$

ξ, α, and K are parameters of the GLO distribution estimated from L-moments. ξ describes the location along the GLO distribution and can be interpreted as a median depth for a given duration. α and K describe the scale and shape of the GLO distribution, respectively. X_d refers to the precipitation depth for a given duration. K is dimensionless while ξ, α, and X_d have units of inches. Asquith (1998) contains iso-maps of the state displaying K, ξ, and α values, which vary by duration and location.

Table 1 shows return periods for a point (T) at various durations using the stage IV bins. The maximum return period was approximately 320 years at the 6 h duration. Return periods at a point would be somewhat higher than shown here since these are derived from 4 km × 4 km radar averages. Several point estimates (rain gauges) operating as part of the Community Collaborative Rain, Hail & Snow Network (CoCoRaHS; www.cocorahs.org; Cifelli et al., 2005) captured 24 h accumulations from the event. The maximum twenty four hour return period from CoCoRaHS was 270 years. If it is assumed this amount fell during a 12 h period (which the radar data suggests), the return period is 380 years. No sub-daily rain gauges apart of a formal network are known to have captured the event in the basin.

It should be noted that while the return periods imply very rare rainfall from the storm event, accumulations in excess of 250 mm are not particularly rare when the Texas Hill Country is considered as a whole. Examining just the previous five years, multiple storms along the Balcones Escarpment can be identified exceeding this threshold (9 June 2010, 31 October 2013, 25 May 2013; Nielsen et al., 2016) (7 September 2010; Furl et al., 2015) (30 October 2015).

5. Flood hydrology

5.1. Empirical record

Three USGS gauging stations and one Edwards Aquifer Authority (EAA) station were operating in the basin during the flood event (Fig. 2). Full stage hydrographs were recorded at an EAA station located mid-basin (upmost gauging station; 675 km^2) along with a USGS gauging station at the outlet (USGS 08171350–1129 km^2). Partial discharge hydrographs were collected by the two interior USGS stations separated by a short distance in the lower portion of the basin (USGS 08171300 (Kyle) – 1067 km^2; USGS 08171000 (Wimberley) – 920 km^2). Both of the flow measuring gauges failed during the rising limb of the hydrograph. Fig. 6 shows the data collected by the gauging stations.

The rainfall runoff data indicate a very rapid stream flow response with a steep, sharp crested hydrograph measured in the middle

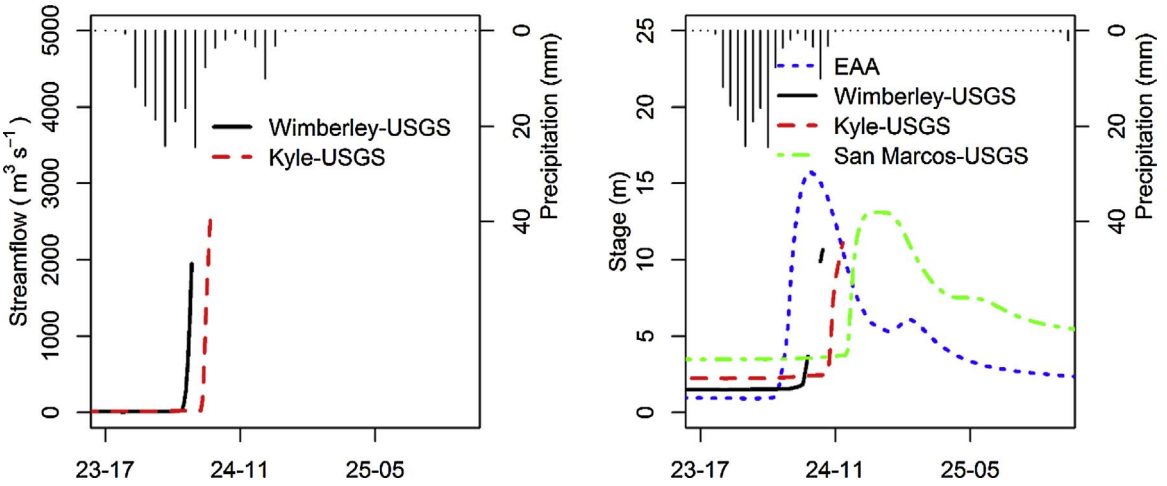

Fig. 6. Stream flow (left) and stage (right) data collected during the event. Gauge locations are shown in Fig. 2.

portion of the basin. At the EAA gauging location, the river rose over 8 m in one hour. Lag times (defined here as time difference between peak discharge and the time centroid of basin averaged rainfall) were calculated for the two locations with full stage hydrographs. Rainfall for the seven hour maximum (1900 23 May–0200 24 May) were clipped to the drainage areas of the gauging stations, and we assumed a uniform hourly rainfall rate when calculating the time centroid of the basin's rainfall. Lag time at the upstream gauge was estimated at 5.5 h (+/− 15 min − gauge reporting increment) and 11.41 h at the watershed outlet (+/− 5 min –gauge reporting increment).

The USGS estimated peak flows at the Wimberley station (USGS 08171000) using indirect slope area techniques. Peak discharge was estimated at 4955 m^3/s with a stage estimate of 13.7 m making it the flood of record for this gauge with measurements dating back to the 1920s. Flow recurrence intervals were calculated at this station using the methods outlined by the USGS PeakFQ program (Flynn et al., 2006). PeakFQ provides statistical flood frequency analysis of annual-maximum peak flows following the log-Pearson Type III frequency distribution. Parameters of the frequency distribution are estimated from the logarithmic sample moments (mean, standard deviation, and coefficient of skewness) of the record of annual peak flows, with adjustments for low outliers, high outliers, historic peaks, and generalized peak skew.

Supplementary Fig. A7 displays recurrence intervals for a given flow bracketed with 95% confidence intervals along with annual peak flows. The recurrence intervals (x-axis) correspond to the inverse of the exceedance probabilities calculated in accordance with the PeakFQ methodology (Flynn et al., 2006). The curve displayed in the top panel includes the May 2015 peak flow in the calculations while the bottom panel omits the peak flow. When the May 2015 peak flow is included in the dataset, the recurrence interval for the May 2015 flood is 178 years. When the curve is constructed without the May 2015 data point, the USGS indirect estimate represents a recurrence interval of approximately 379 years. It's worth noting, the probable maximum flood for a basin this size in this region of Texas is estimated at 17,000 $m^3 s^{-1}$ (Asquith and Slade, 1995).

5.2. GSSHA simulations

5.2.1. Model setup

The May 2015 flood event was simulated with the GSSHA model (Downer and Ogden, 2004), and hydrological processes simulated included infiltration, landscape retention, 2-D overland flow, and 1-D stream routing. Evapotranspiration and deep aquifer contributions were not included. Model preprocessing was conducted using ArcGIS and Aquaveo's Watershed Modeling System (EMRL, 2016). Watershed terrain was constructed from USGS 10 m DEMs filled using the Cleandam algorithm distributed with the GSSHA model. The USGS gauging station at San Marcos, TX (USGS 08171350) served as the outlet. Land use and land cover data were extracted from the National Land Cover Dataset (Homer et al., 2015). Soils data were prepared from Natural Resources Conservation Service datasets (Soil Survey, 2013) along with maps from the EAA (Edwards Aquifer Authority, 2015) defining the Edwards Aquifer recharge zone.

Infiltration calculations were conducted using Green and Ampt with redistribution (Ogden and Saghafian, 1997) and initial saturated hydraulic conductivity values provided by Rawls et al. (1983). Grid cells were assigned to one of 4 land use classes for retention and overland roughness parameterization. As discussed in the introduction, heavy rainfall in the months leading to the event left very moist soils. Initial soil moistures were set at 0.3 (cm^3/cm^3) representing very moist conditions (up to 80% volumetric water content).

Stream channels were modeled using irregular cross sections for the main channel and large tributaries. Channel and floodplain geometry were extracted from a triangular irregular network constructed from the DEM. Flood plain geometry was extracted with the channels allowing for control of floodplain simulation. Upland tributaries were modeled as a uniform trapezoidal profile. Reach specific Manning's n values were assigned based on field observations (~125 river sites visited) and prior modeling experience in this region of Texas (Sharif et al., 2010a; Sharif et al., 2010b; Sharif et al., 2013; Elhassan et al., 2013; Chintalapudi et al., 2014).

Routing was calculated using the diffusive wave equation in 1D for streams and 2D for overland flow. The model was run on a 150 m grid with a 1 min time step. Model performance was assessed using the commonly applied r^2, Nash-Sutcliffe efficiency (NSE), and percent bias (PBIAS) measures (Moriasi et al., 2007).

5.2.2. Model calibration and validation

Measured flow and stage IV precipitation data were collected for 6 storms for model calibration and validation. Flow performance was examined at the Wimberley USGS gauge, and is the primary focus of our analysis since indirect flow estimates are available. The GSSHA model was calibrated to a single storm event occurring 17–18 November 2004 with the remaining 5 events used to validate the model. Calibration was performed manually with saturated hydraulic conductivity, channel geometry, channel roughness, and overland roughness showing the most sensitivity. Table 2 shows calibrated surface parameters used in the final model run.

The calibration event produced peak flows of approximately one fifth of the May 2015 event at Wimberley. Although other storms in the dataset produced peak flows greater than the calibration storm event, it was chosen due to the spatial organization of the rainfall and antecedent conditions. The 17–18 November 2004 storm was centered in the upper portion of the basin straddling the Little Blanco and Upper Blanco watersheds. The May 2015 event contained very similar aerial rainfall coverage across the upper portion of the watershed. The two October events producing the highest peak flows were centered just upstream of the Wimberley stream gauge. Visual observations and high water mapping at approximately 125 river locations after the May 2015 event indicated complicated river hydraulics in the upper portion of the basin that would have significantly affected the floodwave. Essentially, flood waters passed through a series of confining canyons and open flood plains between the towns of Blanco and Wimberley. River stage from the May 2015 event varied by more than 8 m in this section of the river depending on the surrounding channel geometry (Furl-

Table 2
GSSHA infiltration and overland flow parameters.

Soil texture/Land use	Saturated hydraulic conductivity (cm h^{-1})	Capillary head (cm)	Effective porosity	Manning's roughness coefficient	Retention (mm)
Recharge zone	10	23.6	0.417	–	–
Clay	1.2	0.06	0.385	–	–
Loam	0.01	1.3	0.434	–	–
Fine loam	0.02	2.18	0.412	–	–
Fine silt	0.01	0.68	0.486	–	–
Fine sand	0.03	23.6	0.417	–	–
Urban	–	–	–	0.18	5
Forest	–	–	–	0.25	5
Shrub	–	–	–	0.2	5
Grassland/Agriculture	–	–	–	0.3	5

unpublished data). In addition to the spatial location of the rainfall, the November 17–18 2004 event occurred at the tail end of significant rainfall across the area. Rain gauges in the neighboring basin to the north recorded rainfall in excess of 100 − 150 mm in the days leading up to the validation event (LCRA, 2016).

Measured and simulated hydrographs at the Wimberley gauge along with model performance statistics are shown in Fig. 7 and Table 3, respectively. The calibration event performed well with NSE and r^2 values ≥0.9 and PBIAS near 10%. The model performed well for the 22–24 November 2004 event, but overestimated volume for the remaining runs (31 October 2013; 30 October 2015; 08–09 September 2010; 25–26 May 2013. The two worst performing validation events (08–09 September 2010; 25–26 May 2013) significantly overestimated flows and were fairly low flow events compared to the calibration run. Overestimations of these events are likely related to antecedent soil moisture conditions which are discussed below.

5.2.3. May 2015 simulation

Results from the May 2015 event simulation are shown in Fig. 8. The modeled floodwave presents itself as a sharp crested peak and appears similar to the stage hydrograph recorded at the EAA gauge upstream. Modeled peak flows at the Wimberley gauge and basin outlet were 4780 m^{3}s^{-1} and 4072 m^{3}s^{-1}, respectively. Simple percent error in peak flows between modeled values and the USGS indirect estimate were less than 5%.

Runoff ratios were calculated for each of the 6 calibration/validation events at the Wimberley gauge in order to provide comparison with the May 2015 event (Table 4). The ratios were calculated from stage IV data clipped to the Wimberley gauge watershed and measured flows from the gauging station. The runoff volume from the May 2015 event were calculated from the GSSHA output.

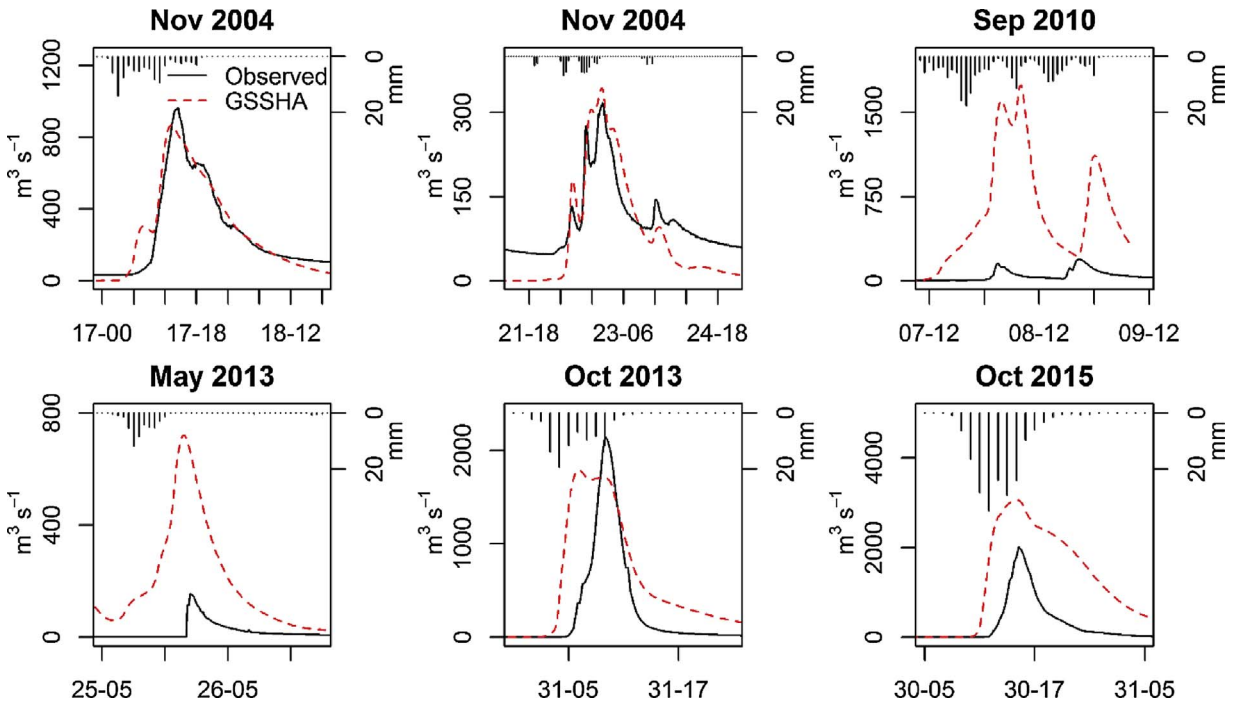

Fig. 7. Calibration and validation hydrograph plots for the GSSHA model at the USGS gauge in Wimberley, Tx. X-axis indicates day-hour.

Table 3
GSSHA model performance statistics.

Storm event	r^2	NSE	PBIAS (%)
17–18 November 2004	0.91	0.90	10.2
23–24 November 2004	0.84	0.48	−3.40
September 2010	0.15	−210	1170
May 2013	0.35	−55	988
October 2013	0.61	0.24	106
October 2015	0.65	−4.2	340

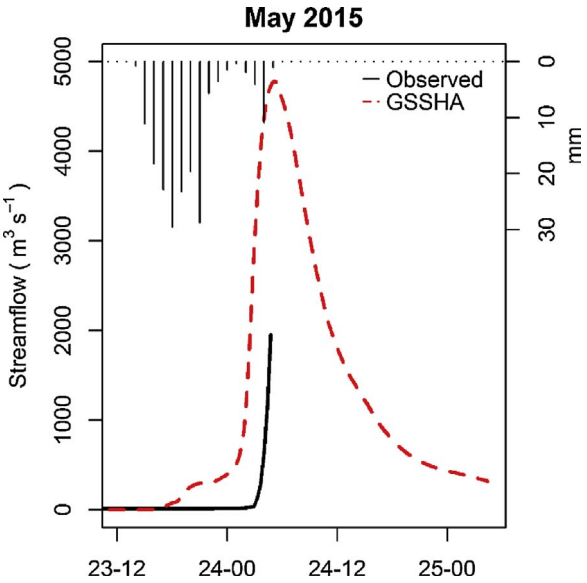

Fig. 8. GSSHA simulation of the May 2015 event at Wimberley plotted with the available USGS gauge data from the location. X-axis indicates day-hour.

Table 4
Storm event runoff ratios.

Storm event	Runoff:Rainfall
17–18 November 2004	0.52
23–24 November 2004	0.58
September 2010	0.05
May 2013	0.07
October 2013	0.35
October 2015	0.12
May 2015	0.69

In an attempt to standardize the calculations across events, runoff volumes were calculated from the start of the rainfall event to 12 h past peak flows. Twelve hours past peak flows provided enough time for hydrographs to return to near baseflow. Runoff ratios ranged an order of magnitude across the events with nearly 10% or less of the rainfall volume exiting the basin for three events (September 2010; May 2013; October 2015) and greater than 50% for three events (17–18 November 2004; 23–24 November 2004; May 2015). The model was calibrated to one of the high runoff ratio events, and model performance was best for other events with increased runoff ratios (23–24 November 2004 and October 2013). The runoff ratio for the May 2015 event was estimated at nearly 70%, although this is likely an overestimation given the volume overestimations for some validation results. Model performance aside, the wide-ranging runoff ratios suggests antecedent conditions combined with spatiotemporal variations in rainfall play a large role in mediating stream response.

The October 2015 event occurred just months after the flood of record for the Wimberley gauge and produced the eight highest peak flow (2010 $m^3 s^{-1}$). The event was centered just upstream of the Wimberley gauge and the stage IV record indicated rainfall volume and rate very close to the May 2015 event (Fig. 9). However, much less water exited the basin with a runoff ratio approximately one fifth of the May 2015 estimate. Soil moisture data were examined from a probe located between Wimberley and San Marcos as part of the COSMOS monitoring network (Freeman Ranch site 57) (Zreda et al., 2012). Data were available for the four most recent storm events (May 2013; October 2013; May 2015; October 2015), and 10 day antecedent soil moisture values are shown

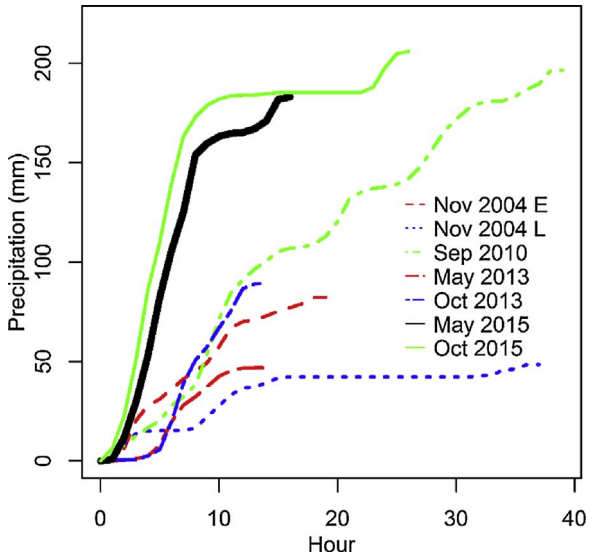

Fig. 9. Rainfall hyetographs developed from stage IV precipitation data for the basin delineated at Wimberley, Tx. Nov 2004 E indicates the "early" November event (17–18 November 2004) and Nov 2004 L indicates the "late" November event (23–24 November 2004).

in Supplementary Fig. A8 . Mean 10 day volumetric soil moisture preceding the May 2015 event was approximately 60% higher than the 10 day period leading up to the October 2013 and 2015 events, and nearly double the May 2013 event. Streamflow volume from the May 2013 event was largely overestimated by the GSSHA model. The effect of soil moisture on model runs was investigated by running the model under varying initial soil moisture conditions ranging from 0.1-0.3 cm^3/cm^3 representing volumetric soil moisture percentages from 25 to 80% (data not shown). The various model representations produced only modest changes to runoff volume and peak flow. The lack of streamflow response to changes in initial soil moisture conditions is a major shortcoming in the GSSHA model setup. However, the model appears to perform reasonably well when antecedent soil moisture is high. Other researchers have documented the varying ability for storm events to produce runoff in the region. In 2009, Smith et al. (2011) documented rainfall in excess of 200 mm with no appreciable flow response in downstream creeks in the Onion Creek drainage basin which borders the Blanco to the north. These results highlight the importance of antecedent conditions and difficulties in building robust hydrologic models that can respond to the soil condition extremes in addition to the heterogeneity of physical features across a basin and channel.

6. Rainfall transpositions

There is much recent interest and research activity in the field of forecasting river flows using QPEs or QPFs (e.g. Liechti et al., 2013), including the recent launch of the United States National Water Model (NOAA NWC, 2016) and opening of the National Water Center. Several numerical weather prediction models are presently available providing near-term fine scale QPFs including the Thunderstorm Identification, Tracking, Analysis and Nowcasting system (Dixon and Wiener, 1993), Tracking Radar Echoes by Correlation (Tuttle and Foote, 1990), and the High Resolution Rapid Refresh model (Benjamin et al., 2016). Forecasting river flows with QPFs has the benefit of providing advanced lead time and some models have the ability to create ensemble forecasts. However, forecast skill is directly related to lead time, and significant errors can arise when attempting to predict rainfall over small, narrow drainages (Vivoni et al., 2007; Sharif et al., 2006). This is particularly problematic in regions like the Texas Hill Country where flood causing precipitation events are often highly localized. QPEs derived from radar and gauge networks have the ability to produce more reliable estimates (e.g. Multi-Radar Multi-Sensor; Zhang et al., 2016), but the maximum theoretical lead time is equal to the basin's time of concentrations.

In this section of the paper, modest perturbations to the position of the storm centroid and intensity of rainfall are created to examine the sensitivity of peak discharge, peak flow timing, and runoff ratios as measured through the GSSHA model simulations at the Wimberley gauge. Rainfall input to the model was varied by displacing the original stage IV grid in 2 km increments up to 24 km. These displacements were done radially in 5° increments. Supplementary Fig. A9 shows the stage IV grid clipped to approximately 25 km. In total, 864 (72 angular shifts * 12 displacements) GSSHA model runs were completed for the original storm. Additionally, the same exercise was completed with a 0.8 and 1.2 multiplier (herein referred to as 0.8 and 1.2 storms) applied to the original precipitation amounts. While the spatial shifts and factor adjustments are arbitrary, they fall well within reasonable ranges of errors expected from QPFs and real time QPEs with no gauge adjustments (Cunha et al., 2013; Bauer et al., 2016).

For a given storm duration and total amount of rainfall over a catchment, the temporal and spatial distributions of the rainfall is controlled by how the storm moved over the catchment. This will have a significant impact on the runoff response of the catchment and the characteristics of the outlet hydrograph (Singh, 1998; Ogden et al., 1995; Roberts and Klingeman, 1970). A storm moving

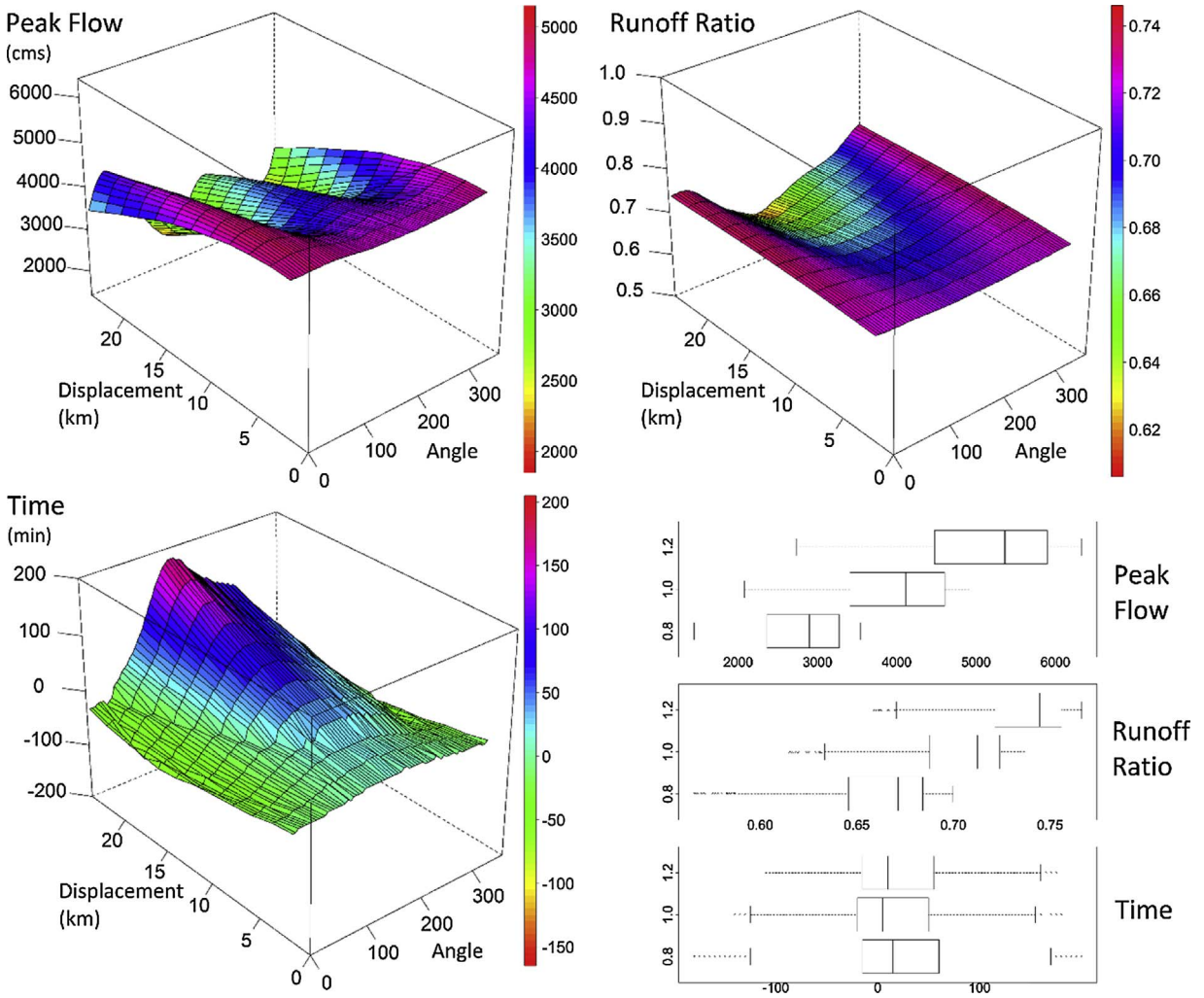

Fig. 10. Three dimensional surfaces of peak flow, runoff ratio, and peak timing versus angle and distance displaced. Plots are for the 1.0 storm. The bottom right panel displays boxplots of values of the 0.8, 1.0, and 1.2 storms.

over a catchment in the upstream direction will result in a hydrograph with a longer base time, a rising limb with a gentler slope, and a smaller peak flow.

6.1. Peak flows, runoff ratios, and peak timing

Peak flows from shifts of the original storm (herein referred to as 1.0 storm) ranged from 2082 to 4915 $m^3 s^{-1}$. Peak discharge from the 1.0 storm with no spatial shift was in the 90th percentile of all 1.0 peak flows. The highest peak discharges from the 1.0 storm typically occurred with 25–50 ° angular shifts and 4–8 km displacements (Fig. 10).

Moving the storm downstream results in attenuated peak flows. An example is provided in Supplementary Fig. A9b by moving the storm along the 340 ° axis a distance of 16 km. In this scenario, we preserve total volume of rainfall above the Wimberley gauge (< 1% difference), but move the epicenter off of the headlands to near the confluence of the rivers. Peak flow at the Wimberley gauge in this scenario is 25% lower (3531 $m^3 s^{-1}$) than the original storm. Runoff ratios remain nearly identical between the scenarios which is not unexpected given the low hydraulic conductivity values of the soils and moist conditions. The effect is similar to having a storm move in the upstream direction rather than downstream (e.g. Ogden et al., 1995). The physical mechanisms responsible for the large difference in hydrograph shape likely results from the steep topography in the uplands and differences in the uplands stream network. Seo (2012) demonstrated that efficient flow networks are much more sensitive to spatial characteristics of a storm.

Maximum flows in the catchment were very sensitive to distance displaced at other angles as well. At 10 km displacements (all angles) flows ranged from 3994 to 4873, and at 20 km displacements the range increased to 2469–4418 (Fig. A10). Stated another way, displacing the storm 20 km the flow recurrence intervals ranged from 34 to 226 years. This in part owes to the narrow shape of the drainage, spatial structure of the storm, and other surface features such as channel morphology and spatial distribution of soils. The timing of peak flows spanned over 5 h for the 1.0 storm with the median time very near the actual peak (+5 min).

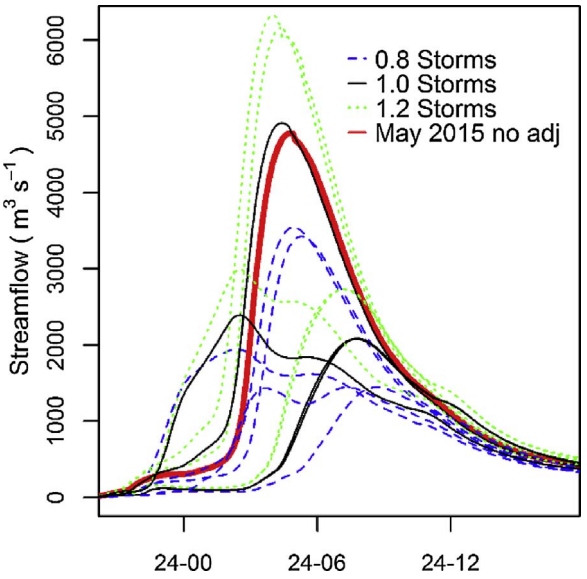

Fig. 11. Ensemble hydrograph plot of maximum and minimum values for peak stream flow and peak timing for the 0.8, 1.0, and 1.2 storm iterations.

Peak flow response to the 0.8 and 1.2 multipliers showed a similar response in terms of storm configuration resulting in minimum and maximum responses. However, there was a non-linear response to the linear adjustments made in the precipitation field. Twenty percent changes in precipitation resulted in approximately 30% changes in median, minimum, and maximum peak flows for the 0.8 and 1.2 storms.

Runoff ratios for the 1.0 storm ranged from 0.61 to 0.74. Including the 0.8 and 1.2 datasets, runoff ratios ranged from 0.56–0.77. While not as wide ranging as the runoff ratios recorded from the six additional storms assessed during model calibration and validation, a maximum difference of 21% highlights the importance of storm location, motion, precipitation amount and distributed soil properties across the basin (Singh, 1998; Ogden et al., 1995; Roberts and Klingeman, 1970).

Visualization of flood forecasts is often performed by displaying an ensemble of hydrographs produced by model output forced by various precipitation forecasts. Ideally, the observed peak discharge will be enveloped by the members creating the ensemble forecast. Fig. 11 shows a hydrograph ensemble of GSSHA output for the undisplaced storms (0.8, 1.0, 1.2) along with the maximum and minimum peak flows and peak timings for each of the three categories.

The ensemble shows a range of shapes from a single peak to a bimodal distribution. Peak flows in the ensemble had a maximum difference of nearly 5000 $m^3 s^{-1}$ peak timings had a range of over six hours. This exercise highlights the difficulty in creating useful flood ensembles in small-medium sized basins from forecasted precipitation.

7. Conclusions

There are three principal conclusions from the work:

- While the synoptic characteristics of intense convective precipitation have been known for decades, and the mescoscale characteristics since the mid-1990s, the advent of high resolution, rapid assimilation and model refresh (e.g., the HRRR), dual-polarization of the WSR-88D network, and high spatial resolution and frequent reporting automated raingauges offers the prospect of short-range, high quality QPF/QPE for input into hydrologic models. But as shown here, even small displacement of QPF/QPE can result in significant differences in hydrograph of resulting flood waves.
- While rainfall amounts from the event were impressive, accumulations from the storm were not uncharacteristic for high magnitude events across the Texas Hill Country. However, the rainfall was able to produce an uncharacteristically large and deadly flood. The entire region had received record to near-record precipitation amounts in the months leading up to the flood. This led to saturated soils and creeks, streams, and rivers primed for maximum rainfall runoff. Analysis of the additional storm events used for hydrological model calibration and validation indicated a wide range of runoff ratios. Runoff ratios for the May 2015 event estimated from the GSSHA model were much larger (≈ 0.7) than other storms examined.
- Rainfall from the event began directly over the headwaters of the basin and were able to remain stationary for many hours. When the most intense rain cells began to move off the headwaters the entire mesoscale convective system moved slowly downstream. Analysis of model iterations of the transposed rainfall fields suggests storm location and motion played a significant role in the peak flows. When the intense headwater cells were started over the middle portion of the basin peak flows were greatly attenuated while volume of runoff remained similar.

Acknowledgements

This work was partially funded by US Army Corps of Engineers Engineer Research and Development Center contract W912H2-16-P-0160 and National Science Foundation RAPID grant 1548215. The authors wish to thank Marcus Gary with the Edwards Aquifer Authority for sharing agency data.

Appendix A. Supplementary data

Supplementary data associated with this article can be found, in the online version, at https://doi.org/10.1016/j.ejrh.2017.12.001.

References

Ashley, S.T., Ashley, W.S., 2008. Flood fatalities in the United States. J. Appl. Meteor. Climatol. 47, 805–818. http://dx.doi.org/10.1175/2007JAMC1611.1.

Asquith, W., Slade, R., 1995. Documented and Potential Extreme Peak Discharges and Relation Between Potential Extreme Peak Discharges and Probable Maximum Flood Peak Discharges in Texas. USGS Water Resources Investigation Report 95–4249, pp. 63pp. http://pubs.usgs.gov/wri/1995/4249/report.pdf.

Asquith, W., 1998. Depth-Duration Frequency of Precipitation for Texas. USGS Water Resources Investigations Report 98–4044, pp. 107pp. http://pubs.er.usgs.gov/publication/wri984044.

Baker, V., 1975. Flood hazards along the balcones escarpment in central texas. Tex. Bur. Econ. Geol. Circular 75-5, 22. http://www.lib.utexas.edu/books/landscapes/publications/txu-oclc-1967634/txu-oclc-1967634.pdf.

Baker, V.R., 1977. Stream–channel response to floods, with examples from central Texas. Geol. Soc. Am. Bull. 88, 1057–1071. http://dx.doi.org/10.1130/00167606(1977)88,1057:SRTFWE.2.0.CO;2.

Bauer, H.S., Schwitalla, T., Wulfmeyer, V., Bakhshaii, A., Ehret, U., Neuper, M., Caumont, O., 2016. Quantitative precipitation estimation based on high-resolution numerical weather prediction and data assimilation with WRF - a performance test. Tellus A 67. http://dx.doi.org/10.3402/tellusa.v67.25047.

Benjamin, S.G., Weygandt, S.S., Brown, J.M., Hu, M., Alexander, C.R., Smirnova, T.G., Olson, J.B., James, E.P., Dowell, D.C., Grell, G.A., Lin, H., Peckham, S.E., Smith, T.L., Moninger, W.R., Kenyon, J.S., Manikin, G.S., 2016. A north american hourly assimilation and model forecast cycle: the rapid refresh. Mon. Wea. Review 144, 1669–1694.

Burnett, J., 2008. Flash Floods in Texas. Texas A&M University Press, pp. 350.

Caracena, F., Fritsch, J., 1983. Focusing mechanisms in the Texas hill country flash floods of 1978. Mon. Wea. Rev. 111, 2319–2332.

Caran, S.C., Baker, V., 1986. Flooding along the balcones escarpment, Central Texas. In: Abbot, P., Woodruff, C. (Eds.), The Balcones Escarpment, Central Texas. Geol. Soc. of Amer., pp. 1–14.

Chintalapudi, S., Sharif, H.O., Xie, H., 2014. Sensitivity of distributed hydrologic simulations to ground and satellite based rainfall. Water 6, 1221–1245. http://dx.doi.org/10.3390/w6051221.

Cifelli, R., Doesken, N., Kennedy, P., Carey, L.D., 2005. The community collaborative rain, hail, and snow network. Bull. Am. Meteorol. Soc. 86 (8), 1069.

Collier, C.G., 2007. Flash flood forecasting: what are the limits of predictability? Quart. J. Roy. Meteor. Soc. 133, 3–23. http://dx.doi.org/10.1002/qj.29.

Collins, E.W., 2004. Summary of the Balcones fault zone, central Texas: a prominent zone of tertiary normal faults marking the western margin of the Texas Coastal Plain. In: Hoh, A., Hunt, B. (Eds.), Tectonic History of Southern Laurentia: a Look at Mesoproterozoic, Late–paleozoic, and Cenozoic Structures in Central Texas. Austin Geological Society Guidebook 24, November 2004, pp. 81–89.

Corfidi, S.F., Merritt, J.H., Fritsch, J.M., 1996. Predicting the movement of mesoscale convective complexes. Weather Forecasting 11, 41–46.

Costa, J.E., 1987. Hydraulics and basin morphometry of the largest flash floods in the conterminous United States. J. Hydrol. 93, 313–338.

Cunha, L.K., Smith, J.A., Baeck, M.L., Krajewski, W.F., 2013. An early performance evaluation of the NEXRAD dual-polarization radar rainfall estimates for urban flood applications. Weather Forecasting 28, 1478–1497. http://dx.doi.org/10.1175/WAF-D-13-00046.1.

Dixon, M.J., Wiener, G.M., 1993. TITAN: thunderstorm identification, tracking, analysis, and nowcasting-a radar-based methodology. J. Atmos. Oceanic Technol. 10, 785–797. http://dx.doi.org/10.1175/1520-0426(1993)010%3C0785:TTITAA%3E2.0.CO;2.

Doswell, C.A., Brooks, H.E., Maddox, R.A., 1996. Flash flood forecasting: an ingredients-based methodology. Weather Forecasting 11, 560–581.

Downer, C.W., Ogden, F.L., 2004. GSSHA: model to simulate diverse stream flow producing processes. J. Hydrol. Eng. 9, 161–174.

EMRL, 2016. Watershed Modeling System (WMS) Version 10.0 Tutorial. Brigham Young University, Environmental Modeling Research Laboratory, Utah.

Edwards Aquifer Authority, 2015. Aquifer Zones. (Accessed 6 June 2015). http://www.edwardsaquifer.org/aquifer-data-and-maps/maps.

Elhassan, A., Sharif, H.O., Jackson, T., Chintalapudi, S., 2013. Performance of a Conceptual and a Physically-Based Model in Simulating the Response of a Semi-Urbanized Watershed in San Antonio, Texas. Hydrol. Processes 27, 3394–3408. http://dx.doi.org/10.1002/hyp.9443.

Flynn, K.M., Kirby, W.H., Hummel, P.R., 2006. User's Manual for Program PeakFQ, Annual Flood Frequency Analysis Using Bulletin 17 B Guidelines. U.S. Geological Survey Techniques and Methods Book 4, Chapter B4. pp. 42. http://water.usgs.gov/software/PeakFQ/.

Fulton, R.A., Breidenbach, J.P., Seo, D.J., Miller, D.A., O'Bannon, T., 1998. The WSR-88D rainfall algorithm. Weather Forecasting 13, 377–395. http://dx.doi.org/10.1175/1520-0434(1998)013,0377:TWRA.2.0.CO;2.

Furl, C., Sharif, H.O., El Hassan, A., Mazari, N., Burtch, D., Mullendore, G.L., 2015. Hydrometeorological analysis of tropical storm hermine and central Texas flash flooding, september 2010. J. Hydrometeor. 16, 2311–2327.

Grice, G.K., Maddox, R.A., 1983. Synoptic characteristics of heavy rainfall events in South Texas. Natl. Weather Dig. 8, 8–16.

Grimshaw, T.W., Woodruff, C.M., 1986. In: Abbott, P.L., Woodruff, C.M. (Eds.), Structural Style in an En Echelon Fault System, Balcones Fault Zone, Central Texas. Geomorphologic and Hydrologic Implications. The Balcones escarpment. Geological Society of America, Central Texas, pp. 71–76.

Homer, C.G., Dewitz, J.A., Yang, L., Jin, S., Danielson, P., Xian, G., Coulston, J., Herold, N.D., Wickham, J.D., Megown, K., 2015. Completion of the 2011 National Land Cover Database for the conterminous United States-Representing a decade of land cover change information. Photogramm. Eng. Remote Sens. 81, 345–354.

LCRA, 2016. Lower Colorado River Authority Hydromet. http://hydromet.lcra.org/full.aspx.

Liechti, K., Panziera, L., Germann, U., Zappa, M., 2013. The potential of radar-based ensemble forecasts for flash-flood early warning in the southern Swiss Alps. Hydrol. Earth Syst. Sci. 17, 3853–3869.

Lin, Y., Mitchell, K.E., 2005. The NCEP stage II/IV hourly precipitation analyses: development and applications. In: 19th Conf. on Hydrology. San Diego, CA, Amer. Meteor. Soc., 1.2.. . https://ams.confex.com/ams/pdfpapers/83847.pdf.

Looper, J.P., Vieux, B.E., 2012. An assessment of distributed flash flood forecasting accuracy using radar and rain gauge input for a physics-based distributed hydrologic model. J. Hydrol. 412–413 (114–132). http://dx.doi.org/10.1016/j.jhydrol.2011.05.046.

Moriasi, D.N., Arnold, J.G., Van Liew, M.W., Bingner, R.L., Harmel, R.D., Veith, T.L., 2007. Model evaluation guidelines for systematic quantification of accuracy in watershed simulations. T. ASABE 50, 885–900.

Nelson, B.R., Prat, O.P., Seo, D.J., Habib, E., 2015. Assessment and implications of NCEP stage IV quantitative precipitation estimates for product intercomparisons. Weather Forecasting 31, 371–394.

Nielsen, E.R., Schumacher, R.S., Keclik, A.M., 2016. The effect of the balcones escarpment on three cases of extreme precipitation in Central Texas. Mon. Weather Rev. 144, 119–138.

Nielsen-Gammon, William, J., 2012. The 2011 Texas drought. Texas Wat. J. 3, 59–95.

Nielsen-Gammon, J.W., Zhang, F., Odins, A.M., Myoung, B., 2005. Extreme rainfall in Texas: Patterns and predictability. Phys. Geog. 26, 340–364.
NOAA NWC, 2016. The National Water Model. http://water.noaa.gov/about/nwm.
NOAA/NWS/Storm Prediction Center, 2016. SPC Severe Weather Events Archive. http://www.spc.noaa.gov/exper/archive/events/.
NOAA National Centers for Environmental Information, 2016. Climate Division Precipitation Archives. (Accessed 1 March 2016). http://www1. ncdc.noaa.gov/pub/data/cirs/climdiv/.
Ogden, F.L., Richardson, J.R., Julien, P.Y., 1995. Similarity in catchment response 2. Moving rainstorms. Water Resour. Res. 31, 1543–1547.
Ogden, F.L., Saghafian, B., 1997. Green and Ampt infiltration with redistribution. J. Irrig. Drain. 123, 386–393. http://dx.doi.org/10.1061/(ASCE)0733-9437(1997)123:5(386).
Orlanski, I., 1975. A rational subdivision of scales for atmospheric processes. Bull. Am. Met. Soc. 56, 527–530.
Patton, P.C., Baker, V.R., 1976. Morphometry and floods in small drainage basins subject to diverse hydrogeomorphic controls. Water Resour. Res. 12, 941–952. http://dx.doi.org/10.1029/WR012i005p00941.
Rawls, W.J., Brakensiek, D.L., Miller, N., 1983. Green-Ampt infiltration parameters from soils data. J. Hydraul. Eng. 109, 62–70. http://dx.doi.org/10.1061/(ASCE)0733-9429(1983)109:1(62).
Roberts, M.C., Klingeman, P.C., 1970. The influence of landform and precipitation parameters on flood hydrographs. J. Hydrol. 11, 393–411.
Schroeder, A., Basara, J., Shepherd, J.M., Nelson, S., 2016. Insights into atmospheric contributions to urban flash flooding across the United States using an analysis of rawinsonde data and associated calculated parameters. J. App. Met. Climol. 55, 313–323.
Seo, Y., 2012. The Effect of Rainstorm Movement on Urban Drainage Network Runoff Hydrographs Ph.D. Dissertation. University of Illinois at urban-Champagne, pp. 215.
Sharif, H.O., Yates, D., Roberts, R., Mueller, C., 2006. The use of an automated now-casting system to forecast flash floods in an urban watershed. J. Hydrometeorol. 7, 190–202. http://dx.doi.org/10.1175/JHM482.1.
Sharif, H.O., Hassan, A.A., Bin-Shafique, S., Xie, H., Zeitler, J., 2010a. Hydrologic Modeling of an extreme flood in the Guadalupe river in Texas. J. Am. Water Res. 46, 881–891. http://dx.doi.org/10.1111/j.1752-1688.2010.00459.x.
Sharif, H.O., Sparks, L., Hassan, A.A., Zeitler, J., Xie, H., 2010b. Application of a distributed hydrologic model to the november 17, flood of bull creek watershed, Austin, Texas. J. Hydrol. Eng. 15, 651–657. http://dx.doi.org/10.1061/(ASCE)HE.1943-5584.0000228.
Sharif, H.O., Hossain, M., Jackson, T., Bin-Shafique, S., 2012. Person-place-time analysis of vehicle fatalities caused by flash floods in Texas. Geomatics Nat. Hazards Risk 3, 311–323. http://dx.doi.org/10.1080/19475705.2011.615343.
Sharif, H.O., Chintalapudi, S., Elhassan, A., Xie, H., Zeitler, J., 2013. Physically-based hydrological modeling of the 2002 floods in San Antonio, Texas. J. Hydrol. Eng. 18, 228–236. http://dx.doi.org/10.1061/(ASCE)HE.1943-5584.0000475.
Sharif, H.O., Jackson, T., Hossain, M., 2014. David zane analysis of flood fatalities in texas. Nat. Hazard. Rev. 16. http://dx.doi.org/10.1061/(ASCE)NH.1527-6996.0000145.
Singh, V.P., 1998. Effect of the direction of storm movement on planar flow. Hydrol. Process. 12, 147–170.
Smith, B.A., Hunt, B.B., Andrews, A.G., Watson, J.A., Gary, M.O., Wierman, D.A., Broun, A.S., 2015. Surface water-groundwater interactions along the Blanco River of central Texas, USA. Environ. Earth Sci. 74, 7633–7642.
Smith, B., Hunt, B., Beery, J., 2011. Final Report for the Onion Creek Recharge Project, Northern Hays County, Texas. Barton Springs/Edwards Aquifer Conservation District, Austin, TX, pp. 134. http://www.bseacd.org/uploads/319h%20Onion%20Creek%20Final%20Report%208_15_11_web.pdf.
Smith, B.A., Hunt, B.B., Andrews, A.G., Watson, J.A., Gary, M.O., Wierman, D.A., Broun, A.S., 2014. Hydrogeologic influences of the blanco river on the trinity and edwards aquifers, Central Texas, USA. In: Andreo, B., Carrasco, F., Duran, J.J., Jimenez, P., Lamoreaux, J.W. (Eds.), Hydrogeological and Environmental Investigations in Karst Systems. Springer Environmental Earth Sciences, pp. 153–161.
Smith, J.A., Baeck, M.L., Morrison, J.E., Sturdevant-Rees, P., 2000. Catastrophic rainfall and flooding in texas. J. Hydrometeor. 1, 5–25.
Soil Survey, 2013. Web Soil Survey. NRCS, USDA. (Accessed 6 June 2015). http://websoilsurvey.nrcs.usda.gov/.
Texas Water Development Board, 2015. Texas Reservoirs. (Accessed 31 October 2015). http://waterdatafortexas.org/reservoirs/statewide.
Tuttle, J.D., Foote, G.B., 1990. Determination of the boundary layer airflow from a single Doppler radar. J. Atmos. Ocean. Tech. 7, 218–232.
United States Drought Monitor, 2015. Drought -Categorical Percent Area. (Accessed 31 October 2015). http://droughtmonitor.unl.edu/Home/StateDroughtMonitor.aspx?TX.
Vieux, B.E., Cui, Z., Gaur, A., 2004. Evaluation of a physics-based distributed hydrologic model for flood forecasting. J. Hydrol. 298, 155–177.
Vivoni, E.R., Entekhabi, D., Hoffman, R.N., 2007. Error propagation of radar rainfall nowcasting fields through a fully distributed flood forecasting model. J. Appl. Meteor. Climatol. 46, 932–940.
Wang, S.-Y.S., Huang, W.-R., Hsu, H.-H., Gilles, R.R., 2015. Role of the strengthened El Niño teleconnection in the May 2015 floods over the southern Great Plains. Geophys. Res. Lett. 42, 8140–8146. http://dx.doi.org/10.1002/2015GL065211.
Wilcox, B.P., Wilding, L.P., Woodruff, C.M., 2007. Soil and topographic controls on runoff generation from stepped landforms in the Edwards Plateau of Central Texas. Geophys. Res. Lett. 34, 1–6. http://dx.doi.org/10.1029/2007GL030860.
Zahran, S., Brody, S., Peacock, W., Vedlitz, A., Grover, H., 2008. Social vulnerability and the natural and built environment: a model of flood casualties in Texas. Disasters 32, 537–560. http://dx.doi.org/10.1111/j.1467-7717.2008.01054.x.
Zhang, J., Howard, K., Langston, C., Kaney, B., Qi, Y., Tang, L., et al., 2016. Multi-radar multi-sensor (MRMS) quantitative precipitation estimation: initial operating capabilities. Bull. Am. Meteorol. Soc. 97, 621–638.
Zreda, M., Shuttleworth, J., Zeng, X., Zweck, C., Desilets, D., Franz, T., Rosolem, R., 2012. COSMOS: the cosmic-ray soil moisture observing system. Hydrol. Earth Syst. Sci. 16, 4079–4099. http://dx.doi.org/10.5194/hess-16-4079-2012.